

Comparison of Special Sensor Microwave Imager and buoy-measured wind speeds from 1987 to 1997

C. A. Mears, Deborah K. Smith, and Frank J. Wentz

Remote Sensing Systems, Santa Rosa, California

Abstract. We compare wind speeds derived from microwave radiometer measurements made by the Special Sensor Microwave Imager (SSM/I) series of satellite instruments to those directly measured by buoy-mounted anemometers. The mean difference between SSM/I and buoy winds is typically $<0.4 \text{ m s}^{-1}$ when averaged over all operational Tropical Atmosphere-Ocean and National Data Buoy Center buoys for a given year, and the standard deviation is $<1.4 \text{ m s}^{-1}$. Mean errors for a given satellite-buoy pair typically range from -1 to $+1 \text{ m s}^{-1}$, with standard deviations $<1.4 \text{ m s}^{-1}$. Two methods of converting buoy-measured wind speed to a standard value measured at a height of 10 m are compared. We find that the principal difference between a simple logarithmic correction and a more detailed conversion to 10 m equivalent neutral stability wind speed is a shift of wind speed by about 0.12 m s^{-1} with no change in the distribution of SSM/I-buoy wind speed differences.

1. Introduction and Motivation

The use of well-calibrated satellite-based microwave radiometers makes it possible to obtain long time series of geophysical parameters. Over the oceans these parameters include air temperature, the three phases of atmospheric water, near-surface wind speed, sea surface temperature, and sea ice type and concentration. The measurements in turn enable a wide variety of studies of hydrological [Chou *et al.*, 1995, 1996, 1997] processes and can improve weather prediction via data assimilation into operational models [Ardizzone *et al.*, 1996; Deblonde *et al.*, 1997; Deblonde and Wagneur, 1997; Ledvina and Pfaendtner, 1995]. In order for these studies to be meaningful and accurate it is important that the satellite-derived geophysical quantities are compared with surface measurements of the same quantities to characterize the overall accuracy and precision of the satellite-derived data set.

In this paper we present a detailed and comprehensive comparison between sea surface winds derived from microwave measurements made using the Special Sensor Microwave Imager (SSM/I) series of instruments and estimates of wind speed made by a large set of buoys moored in a number of regions in the world's oceans. While other comparisons of SSM/I wind speeds to in situ measurements and modeled wind speeds have been made [Boutin and Etcheto, 1996; Boutin *et al.*, 1996; Busalacchi *et al.*, 1993; Esbensen *et al.*, 1993; Halpern, 1993; Waliser and Gautier, 1993], most of these have been made using SSM/I results computed using earlier, less accurate algorithms and have reported results for at most, only the first two satellites in the series. Since the later satellites in the series were calibrated indirectly by comparing their results with those from earlier satellites at the antenna temperature level, it is important to compare the geophysical parameters produced by later satellites against in situ data. In this work we compare the wind speed results from the first four past and currently operating SSM/I instruments with buoy data. We exclude satellite F14

from the comparison since it has not yet undergone detailed intercalibration with the previous satellite.

In section 2 we describe the SSM/I data set, including a short summary of the wind retrieval algorithm, the range of dates over which data are available from each satellite in the SSM/I series, and the criteria we used to select data for the comparison with the buoy data. In section 3 we discuss the buoy data set, including a short description of the various buoys, their location, and the time periods over which data are available. In section 4 we describe our method for producing SSM/I-buoy-collocated data points. In section 5 we describe the two procedures we used to adjust the buoy wind speeds, which are measured at a variety of heights, to a standard wind speed at a height of 10 m. In section 6 we report a detailed comparison between SSM/I and buoy wind speeds. In section 7 we compare the impact of the two wind speed correction routines discussed in section 5 to the SSM/I-buoy comparison process, and in section 8 we discuss the origin and magnitudes of the errors in both the SSM/I and buoy wind speeds.

2. Summary of the SSM/I Data Set

The SSM/I [Hollinger *et al.*, 1987] is a series of Earth-observing multiband microwave radiometers operating on Defense Meteorological Satellite Program (DMSP) polar orbiters. The first SSM/I instrument flew on the DMSP F08 spacecraft from 1987 to 1991. Since then, four subsequent SSM/I instruments have been successfully launched and operated on later DMSP orbiters. Table 1 shows the period of valid data for each of the SSM/I instruments. The orbit for each satellite is near-circular, Sun synchronous, and near-polar, with an inclination of 98.8° . The altitude of the orbit is $860 \pm 2 \text{ km}$, and the orbital period is $\sim 102 \text{ min}$.

The SSM/I instrument consists of seven radiometers sharing a common feedhorn. Dual-polarization measurements are made at 19.35, 37.0, and 85.5 GHz, and a single vertical polarization measurement is made at 22.235 GHz. Earth observations are made during a 102.4° segment of each scan, corresponding to a 1400 km swath on the Earth's surface. Complete

Copyright 2001 by the American Geophysical Union.

Paper number 1999JC000097.
0148-0227/01/1999JC000097\$09.00

Table 1. Time Period of Valid Data for Each SSM/I Instrument

Satellite	Begin Date	End Date
F08	July 1987	December 1991
F10	January 1991	November 1997
F11	January 1992	present
F13	May 1995	present
F14	May 1997	present

coverage of the Earth is provided every 2 or 3 days, except for small patches near the poles.

Using these observations, it is possible to retrieve three important geophysical parameters over the oceans. These parameters are the near-surface wind speed, the columnar water vapor, and the columnar cloud liquid water L . The rainfall rate can also be inferred, but in this paper we restrict our investigation to areas without rain. The physical basis for these retrievals is the absorption and scattering of microwaves by water in the atmosphere and the roughening of the ocean surface by wind stress, which changes its emission and reflection properties. The algorithm used for this work is described in detail elsewhere [Wentz, 1997]. It is important to note that since the satellite measures the surface roughness, the property of the wind that is most directly measured is the stress. This is converted to a wind speed assuming that the boundary layer over the ocean is neutrally stable.

The Wentz [1997] algorithm was chosen by NASA for the production of the Scanning Multi-channel Microwave Radiometer (SSMR)-SSM/I Pathfinder data set, which will be a 20 year time series of geophysical parameters broadly available to the research community. The data collected and processed to date are available via the internet (<http://www.ssmi.com>) in the form of maps of geophysical parameters on a 0.25° grid. Two maps are available for each valid satellite day, a "morning" map and an "evening" map. The morning map contains data measured during the half of the orbit, from polar region to polar region, that has an equatorial crossing before noon local time, and the evening map contains data from the other half-orbits. Data from these maps were used for all results presented in this work, so that this paper represents a validation of data that is generally available, free of charge, to the research community.

For the purposes of SSM/I-buoy comparison it is important to use only SSM/I wind speed data that is very likely to be free from errors. To do this we reject any of the $0.25^\circ \times 0.25^\circ$ SSM/I pixels that meet any of the following criteria.

1. Any of the eight adjacent pixels is missing or invalid for any reason.
2. Any rain is detected in the central pixel or any of the eight adjacent pixels. If the SSM/I algorithm detects rain in any of the adjacent pixels, it is likely to be raining in at least part of the pixel in question, even if it is below the detection threshold for that pixel.
3. Cloud liquid water >0.18 mm is detected in the central pixel. It is very likely to be raining at a rate below the detection threshold from clouds that are thicker than this cutoff value.

We found that by using these criteria we reduce the number of outlying data points in scatter plots of SSM/I wind speed versus buoy wind speed almost to zero.

3. Buoy Wind Data Set

The buoy wind data set is obtained from the National Data Buoy Center (NDBC) and the Pacific Marine Environmental

Laboratory (PMEL). All available buoy reports from these sources were collected for the period from 1987 through June 1998. Over the period of this study the NDBC operated about 75 moored buoys and 50 C-man stations located in the north-east Pacific, the Gulf of Mexico, the northwest Atlantic, near Hawaii, off the coast of Peru, and in the Marshall Islands. Of these sites we selected 60 stations that are located more than 30 km from the coast. PMEL distributes the data from the Tropical Atmosphere-Ocean (TAO) array [Hayes *et al.*, 1991; McPhaden, 1995] of moored buoys in the equatorial Pacific. For the 1987–1990 period, there are about 20 operational TAO buoys. During the 1991–1992 time period many more TAO buoys become operational, resulting in about 70 TAO buoys by 1993. The period of time over which a given buoy is operational is highly variable because of malfunction and vandalism. No single buoy produced valid wind speed data over the entire time period of this study.

The NDBC uses a variety of buoy types with anemometers mounted either 5 or 10 m above the ocean surface. Wind speed and direction are measured for a period of 8 min each hour, and a scalar average of wind speed and direction is reported. The stated accuracy of wind speed is ± 1 m s⁻¹ with a resolution of 0.1 m s⁻¹ and the stated accuracy of the wind direction is $\pm 10^\circ$ with a resolution of 1.0° [Gilhousen, 1987]. Air temperature is measured at a height of 4 (for buoys with 5 m anemometers) or 10 m (for buoys with 10 m anemometers), and sea surface temperature is measured at a depth of 1.0 or 1.5 m. We have also included a few C-man land-based stations in our "buoy" data set, provided they were mounted on very small islands or reefs. These stations measure wind speed at a variety of heights depending on the nature of the station and only average the data for 2 min each hour. The TAO array uses Atlas buoys, which measure winds for 6 min every hour at a height of 3.8 m with a stated accuracy of 0.3 m s⁻¹ or 3%, whichever is greater, and a resolution of 0.2 m s⁻¹, and the stated accuracy of the wind direction is 5° with a resolution of 1.4° [Mangum *et al.*, 1994] (S. Dickinson *et al.*, unpublished manuscript, 1999). The air temperature is measured at a height of 3.0 m, and the sea surface temperature is measured at a depth of 1 m.

4. Finding Collocated Observations

In order to compare SSM/I wind speeds to those measured by buoys a set of observations collocated both in time and in space must be generated. Each collocated observation for a given satellite-buoy pair was produced using the following procedure. First, for each SSM/I map we check to see if a valid SSM/I observation is spatially collocated with the buoy. Since it is unlikely that the buoy is exactly centered in the SSM/I pixel, the following spatial interpolation procedure is used. Each SSM/I pixel is $0.25^\circ \times 0.25^\circ$. We imagine a square box, 0.15° on a side, centered at the buoy location. If the box is totally within one pixel, the value of the wind speed from that pixel is used. If the buoy is near enough to an edge of its pixel so that the box overlaps two or more pixels, a weighted average is performed of the values in each pixel, with the weights proportional to the areas of the region of the box in each pixel. The value of 0.15 was chosen so that if the buoy is near the center of the SSM/I pixel, only that pixel is used. Interpolation is done if the buoy is near the pixel edge. If any pixel participating in the average fails the data quality criteria discussed in section 2, the observation is not used.

We now have an SSM/I observation collocated with the buoy position. To finish producing a collocated observation, we must produce a buoy observation that occurs at the same time as the SSM/I over flight. We do this by linearly interpolating the buoy observation directly before the over flight and the buoy observation directly after the over flight. Since most buoys in the data set produce data on an hourly basis, the SSM/I over flight time is typically no more than 30 min from the closest buoy observation. If the time difference between the two buoy observations is >120 min, the observation is not used in the comparison.

Collocated observations were generated for each satellite-buoy pair over the entire measurement period of the satellite and buoy. Typically, a year in which both the buoy and the satellite were completely operational resulted in 200–300 collocated observations for the pair.

5. Wind Speed Correction

Satellite-based wind measurements that rely on either microwave scatterometry or radiometry measure the roughness of the ocean surface, which is assumed to be in equilibrium with the wind stress or momentum flux at the ocean surface. Surface observatories, such as buoys, measure the actual wind speed at the height of the anemometer. For buoys this height is typically between 3.8 and 10 m. The relationship between the measured wind speed at a height Z_0 and the wind stress at the surface depends both on Z_0 and on the amount of turbulence occurring between the measuring instrument and the surface. The amount of turbulence is determined by the wind shear and buoyancy of the atmosphere, and the buoyancy is dependent on the density stratification in the atmosphere. Thus conditions that cause identical wind stress, and therefore identical satellite-measured wind speeds, could have different measured wind speeds at a given height. Also, measured wind speeds at different heights would be different from each other, even under identical atmospheric conditions.

Because of these effects, comparing satellite-derived wind speeds directly to buoy-measured wind speeds is certain to lead to large errors. Instead, we convert all buoy-measured winds to a standard height, 10 m. In this work we have used two methods to do this. In the first method we use the simple approach of assuming a logarithmically varying wind profile so that the corrected wind speed at a height z is given by

$$U_{\text{LOG}}(z) = \ln(z/z_0) / \ln(z_m/z_0) * U(z_m),$$

where $U(z)$ is the wind speed at a height z , z_0 is the roughness length, and z_m is the measurement height. This expression can be derived using a mixing length approach assuming neutral stability [Peixoto and Oort, 1992]. The typical oceanic value for z_0 is 1.52×10^{-4} m [Peixoto and Oort, 1992]. Note that this approach does not include effects due to differences in atmospheric stability and therefore may lead to errors when atmospheric conditions differ from neutral stability.

In the second method we convert all buoy wind speed measurements to 10 m neutral stability wind speeds. This is the wind speed that for a given surface stress would be observed at a height of 10 m assuming that the atmosphere is neutrally stable. Thus it can be considered to be a measurement of surface stress expressed in units of wind speed. We have used the method and computer code discussed by Liu and Tang [1996] to do this conversion. This method requires as input

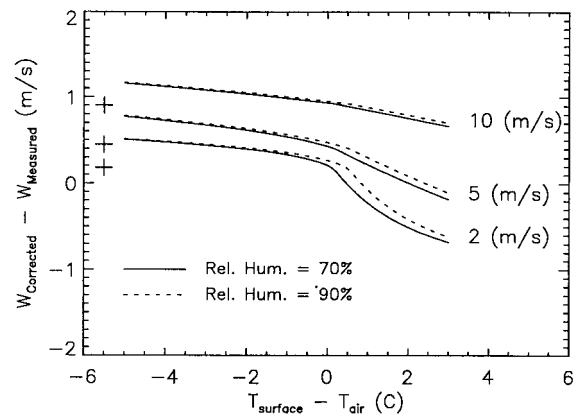


Figure 1. Plot of the correction to 10 m equivalent neutral stability wind as a function of the difference between T_{air} and T_{surface} for three representative wind speeds and two representative values of relative humidity. For this plot the surface temperature is set to 15°C , the atmospheric pressure is set to 1013 mbar and the wind is assumed to be measured at a height of 4 m. The plus signs on the left side of the figure represent the correction calculated using a logarithmic profile for each of the three wind speeds. The logarithmic correction is independent of temperature difference, humidity, and pressure.

data, the measured wind speed u_m at a height z_u , the measured values of sea surface temperature and air temperature at a height z_r , the atmospheric pressure, and the relative humidity measured at a height z_r . For a given buoy measurement many of these data may not be available. If the relative humidity was missing, as was often the case for NDBC buoys, we used a value from a monthly climatology [da Silva et al., 1994]. If the pressure was missing, as was always the case for TAO buoys, we assumed a value 1010 mbar, which is a typical value in the tropics [Peixoto and Oort, 1992]. If either the sea surface temperature or the air temperature was missing, we judged that it was impossible to assess the atmospheric stability and did not use that particular measurement.

In the remainder of this report we will refer to wind speeds corrected to 10 m by the first method as “log-corrected” and those converted to 10 m neutral stability wind speed by the second method as “Liu-corrected.” To show typical magnitudes of these corrections, we plot in Figure 1 the difference between the measured wind speed at 4 m and the Liu-corrected wind speeds as a function of $T_{\text{surface}} - T_{\text{air}}$. Results are plotted for three representative wind speeds (2, 5, and 10 m s^{-1}) and two representative values of the relative humidity (70 and 90%). The surface temperature was assumed to be 15°C , and the atmospheric pressure was assumed to be 1013 mbar. The results are almost independent of atmospheric pressure; changes of 15.0 mbar are not discernable on a plot similar to Figure 1. Logarithmic corrections, which are independent of $T_{\text{surface}} - T_{\text{air}}$, humidity, and pressure, are shown as pluses on the left side of the plot.

To show the typical corrections applied to the buoy wind speeds used for comparison with SSM/I winds, we plot in Figure 2 a scatterplot of the difference between corrected wind speed and measured wind speed as a function of measured wind speed for all over flights by satellite F11 of buoys 52001 and 46003 that had valid data. Buoy 52001 in Figure 2a is in the western tropical Pacific. In this region, there is little variation

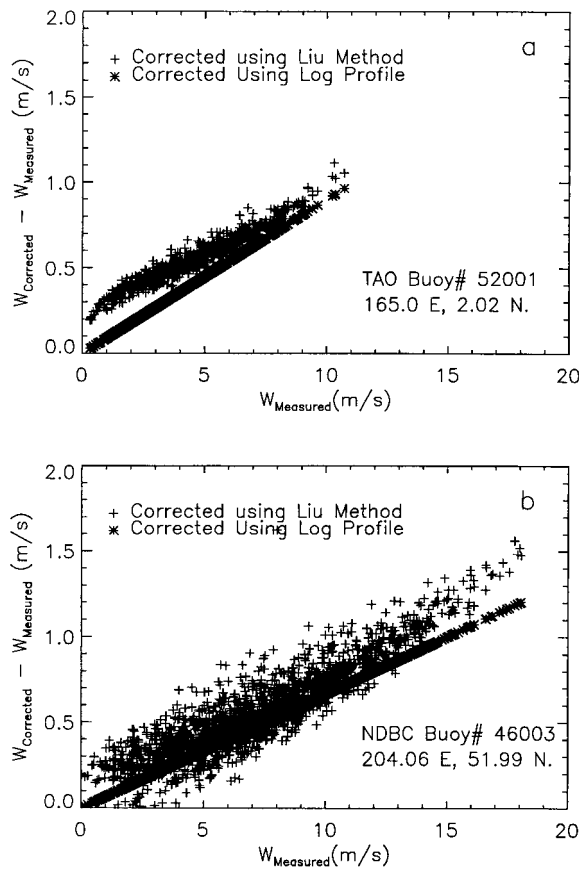


Figure 2. Plot of wind speed correction as a function of measured wind speed for two representative buoys. Both Liu corrections and log corrections are shown for the same set of data. The log corrections lie along a line because they only depend on wind speed and not on the temperature of the air and surface or the relative humidity and pressure as the Liu corrections do.

in temperature, and the sea surface temperature is usually slightly higher than the air temperature. This results in slightly unstable conditions, and the Liu correction is typically a few tenths of a meter per second higher than the log correction. The buoy represented in Figure 2b is in the Gulf of Alaska. Because of its higher latitude and position in the Pacific storm track, this location is subject to much larger variations in the air-surface temperature difference than the site in the tropical Pacific. Both stable and unstable conditions are possible, and values for the Liu correction can be both smaller and larger than the log correction.

In Figure 3 we plot the binned means and standard deviation averages of the difference between log- and Liu-corrected wind speeds. The measurements are divided into bins 0.75 m s^{-1} wide, and the mean and standard deviation are calculated for each bin. The average is made for all buoys in the data set with valid data during over flights of satellite F11. It can be seen from the plot that the main influence of the Liu correction relative to the log correction is to produce a slightly higher wind speed. This bias is largely independent of the buoy-measured wind speed. The mean difference of all observations taken together was 0.12 m s^{-1} , and the standard deviation was 0.17 m s^{-1} . We used 86,780 collocations to produce this plot.

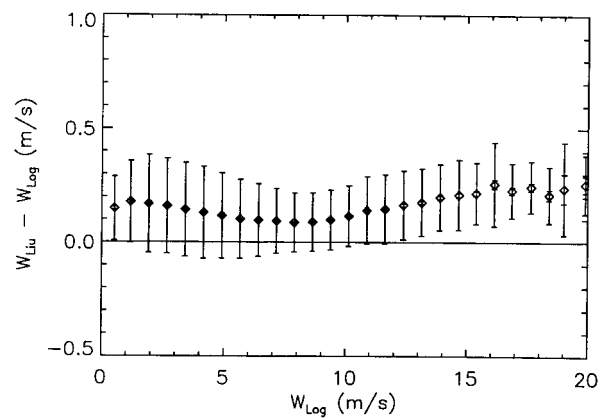


Figure 3. Mean difference between Liu-corrected wind speed and log-corrected wind speed plotted as a function of log-corrected wind speed. Observations were binned into bins 0.75 m s^{-1} wide, and the mean difference is computed. Error bars are ± 1 standard deviation. This plot represents all over flights of satellite F11 with valid data.

6. Comparison of SSM/I and Buoy Wind Speeds

In this section we carry out a comparison of SSM/I and buoy wind speeds using collocated observation pairs gathered using the methods outlined in section 4. We begin by discussing comparisons for two example buoys chosen to represent two distinct regions and atmospheric conditions and then move on to comparisons that use the entire data set. All buoy wind speeds in this section are adjusted to 10 m using the simple logarithmic correction. This is done because the SSM/I algorithm was initially calibrated using log-corrected wind speeds, and we want to perform a comparison to check the consistency and accuracy of the algorithm as calibrated. In section 7 we will address the difference between log-corrected and Liu-corrected wind speeds in greater detail.

In Figure 4a we plot a typical scatterplot of SSM/I-buoy wind speed difference as a function of log-corrected buoy wind speed. These data are from buoy 52001 for every valid over flight by satellite F11 from January 1992 to December 1997. Buoy 52001 is a member of the TAO array and is located at 165.00°E longitude and 2.02°N latitude in the western tropical Pacific. The mean SSM/I wind speed is 0.39 m s^{-1} lower than the log-corrected wind speeds for this satellite-buoy pair, and the overall standard deviation of the wind speed differences is 0.93 m s^{-1} . The absence of data points from the triangular region approximately bounded by a diagonal line of negative unit slope starting at the origin arises from the fact that neither the SSM/I wind speed nor the buoy wind speed is ever reported to be negative. Since the minimum value of the SSM/I wind speed is zero, the minimum value of $W_{\text{SSM/I}} - W_{\text{buoy}}$ is given by $-W_{\text{buoy}}$. The data were then binned into bins 0.75 m s^{-1} wide using the log-corrected buoy wind speed. The mean and standard deviation of the SSM/I-buoy difference was then calculated, and the results are plotted in Figure 4b. The error bars are 1 standard deviation on each side of the mean. The smaller error bars show the standard deviation of the mean, found by dividing the standard deviation for a given bin by the square root of the number of observations in that bin. This plot shows relatively flat behavior, except for an upturn at low wind speed due to the absence of points in the triangular region discussed

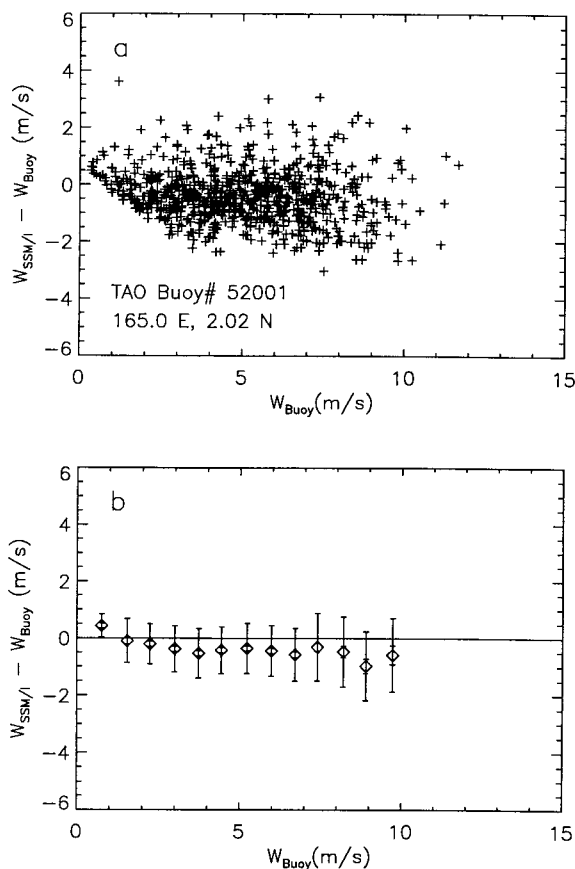


Figure 4. Wind speed difference as a function of buoy wind speed for an example buoy and satellite F11. Buoy wind speeds were corrected to 10 m using a logarithmic profile. (a) A scatterplot. Each symbol corresponds to one buoy-satellite collocated observation. (b) A plot of the binned means. The outer error bars are ± 1 standard deviation, and the inner error bars show the standard deviation of the mean, found by dividing the standard deviation by the square root of the number of observations in the bin.

above. It is important to note that this upturn is a purely statistical effect and is not due to an error in wind speed retrieval at low wind speeds.

Figure 5 is a similar plot for NDBC buoy 44004, located in the northwest Atlantic at 289.63°E longitude and 38.55°N latitude. For this buoy the mean SSM/I wind speed is 0.35 m s^{-1} higher than the log-corrected wind speed, and the overall standard deviation of the differences is 1.66 m s^{-1} . Note that while the mean error of 0.35 m s^{-1} is still small, the standard deviation of 1.66 m s^{-1} is quite a bit larger than it is for the previous case. This is one of the largest standard deviations we found for any satellite-buoy pair. It may be due to large deviations of the sea surface temperature or the water vapor columnar profile from the climatological averages of these parameters that are assumed by the SSM/I wind speed algorithm. The large standard deviation could also be caused by larger variations of wind speed within the SSM/I pixel size, leading to increased collocation error.

We carried out a similar analysis for all buoys with more than 50 valid collocated observations with satellite F11. For each of these 97 buoys we calculate the mean and standard deviation of the difference between collocated SSM/I and buoy

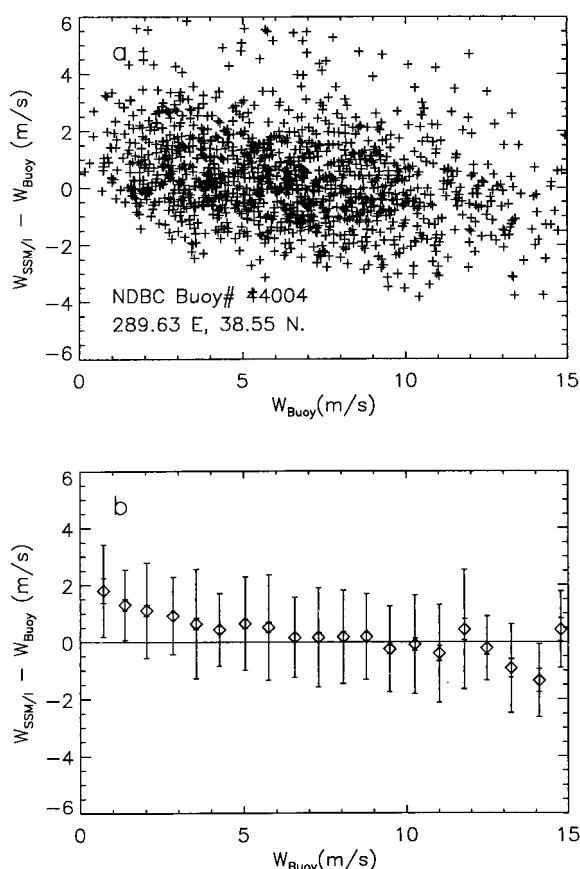


Figure 5. Wind speed difference as a function of buoy wind speed for an example buoy and satellite F11. This figure is similar to Figure 4 except that it is made using data for a buoy in the northwest Atlantic. Note the increased variance in the data.

observations. We also calculated these quantities for the entire buoy data set and for the entire data set on a yearly basis. In Figure 6 we plot the mean error with error bars of ± 1 standard deviation for each buoy. The data have been sorted using the

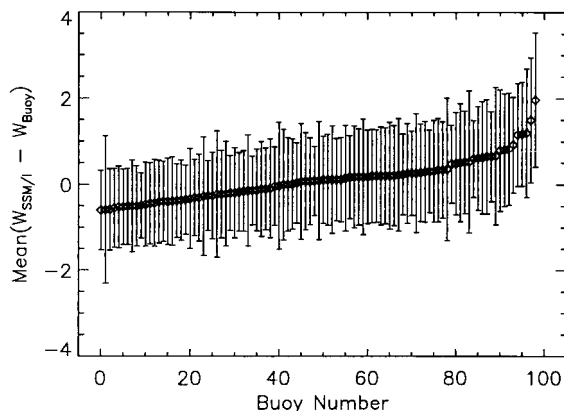


Figure 6. Mean difference between SSM/I wind speed $W_{SSM/I}$ and buoy wind speed W_{buoy} . Error bars are ± 1 standard deviation. The data have been sorted using the mean. The mean difference is $< 1 \text{ m s}^{-1}$ for most buoys with only a few outliers with a larger positive difference.

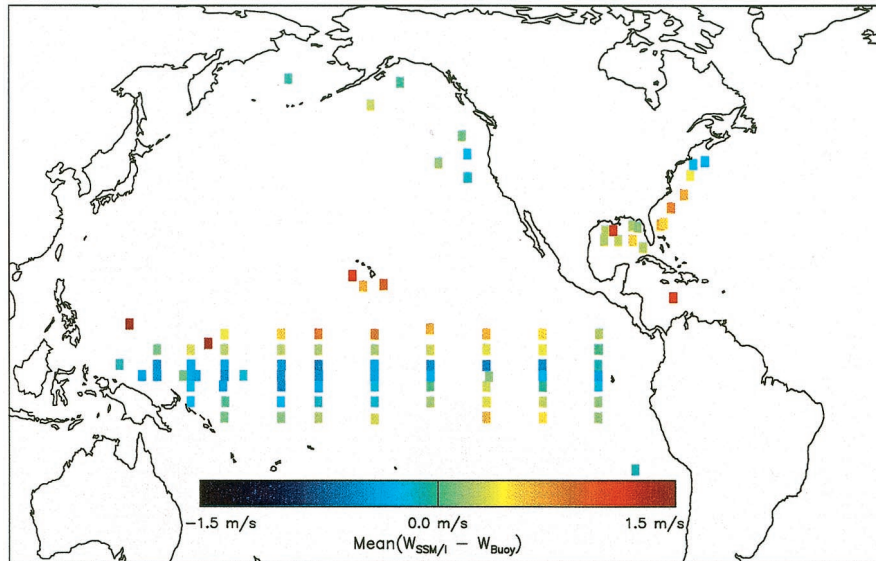


Plate 1. Map of the mean difference between the SSM/I wind speed and the buoy wind speed for all buoys with more than 50 valid collocations for satellite F11.

mean. The overall mean difference, averaged over all buoys, is 0.11 m s^{-1} , with a standard deviation of 1.25 m s^{-1} .

It is also interesting to analyze the geographic distribution of these mean differences. In Plate 1 we plot a color-coded map of these errors on a regional map. Each colored square represents one buoy, and the color of the square represents the mean difference between SSM/I wind speeds and log-corrected buoy wind speeds. For buoys within 5° of the equator the SSM/I wind speeds tend to be too low by $\sim 0.5 \text{ m s}^{-1}$, and for buoys in a band farther from the equator, from 8° to 15° , the SSM/I wind speeds tend to be too high. Even farther from the equator, near the coasts of North America, the trends are less clear. To quantify these results, we show in Table 2 regional averages of mean difference and standard deviation for several regions. The uncertainty of these mean values is found by calculating separately the mean difference for each buoy in the region and then computing the standard deviation of these mean differences divided by the square root of the number of valid buoys in the region. By using this value we are assuming that the mean value for each buoy is an independent measurement of the SSM/I-buoy difference for the given region and reporting the standard deviation of the mean. The South Pacific includes all buoys in the Pacific Ocean south of 4°S latitude, the equatorial Pacific includes all buoys in the Pacific between 4°S and 4°N latitude, the northern tropical Pacific includes all buoys in the Pacific between 4°N and 30°N latitude, the North Pacific includes all buoys in the Pacific north of 30°N , and the North Atlantic includes all buoys in the Atlantic

Ocean and the Gulf of Mexico. Again, the SSM/I wind speeds in the equatorial belt are too low, and those in regions just north and south of this region are too high. Although we only show this pattern for satellite F11, a similar pattern of mean differences occurs for each of the other SSM/I satellites.

The causes of this geographical pattern are not understood at this time. They are probably not related to atmospheric stability since a similar map made using Liu-corrected buoy winds exhibits a nearly identical pattern. Possible causes include differences in sea state for a given wind speed due to differences in fetch or errors due to a systematic dependence of the retrieved SSM/I wind speed on the difference between the wind direction and the direction along which the SSM/I measurement is made. In areas of persistent wind direction, such as the trade winds, this wind direction effect might not average to zero.

In Figure 7 we plot the mean difference between SSM/I wind speed and buoy wind speed as a function of buoy wind speed for all buoys with valid collocated data for satellite F11. Collocated observations were put into bins 0.75 m s^{-1} wide. The mean and standard deviation in each bin are plotted. Figure 7 represents 86,780 collocated observations of SSM/I F11 with a set of 97 buoys. As in Figures 4 and 5, the upturn at low wind speed is primarily a statistical effect and is not due to a bias in the wind retrieval algorithm. Except for this upturn the mean error is $< 1 \text{ m s}^{-1}$ for all wind speeds $< 19 \text{ m s}^{-1}$. Above this speed, there are very few observations (only 31 out of 86,780), so the expected error in the mean in these bins is quite large as

Table 2. Regional Means and Standard Deviations of the SSM/I-Buoy Wind Differences

Region	Mean ($W_{\text{SSM/I}} - W_{\text{buoy}}$)	Standard Deviation ($W_{\text{SSM/I}} - W_{\text{buoy}}$)
South tropical Pacific	0.15 ± 0.06	1.02
Equatorial Pacific	-0.29 ± 0.04	0.97
North tropical Pacific	0.41 ± 0.08	1.26
North Pacific	0.01 ± 0.06	1.33
North Atlantic and Gulf of Mexico	0.20 ± 0.10	1.48

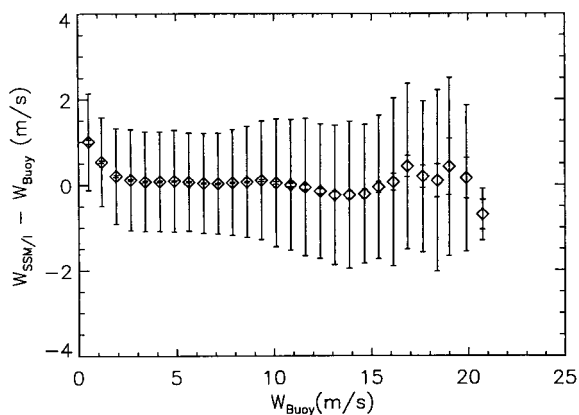


Figure 7. Wind speed difference as a function of buoy wind speed for all buoys and satellite F11. Buoy wind speeds were corrected to 10 m using a logarithmic profile. The collocated observations were sorted into bins 0.75 m s^{-1} wide, and the mean and standard deviation for each bin were calculated. The outer error bars are ± 1 standard deviation, and the inner error bars show the standard deviation of the mean, found by dividing the standard deviation by the square root of the number of observations in the bin.

shown by the inner error bars in the plot. Similar plots were constructed for other satellites. These also showed little systematic error.

Analysis similar to that described above for satellite F11 was performed for the data from each SSM/I satellite launched to date. In addition, a similar analysis was carried out on a year by year basis for each satellite. In Table 3 we report the mean SSM/I—buoy wind speed difference and standard deviation for each satellite, averaged over all years of operation for each satellite. The error estimate for the mean difference is calculated in a way analogous to the procedure used to calculate uncertainties for Table 2. We also report the number of collocated observations over which the average is performed.

In Figure 8 we plot the mean SSM/I—buoy difference as a function of year for each satellite, averaged over all buoys with valid data. The mean error is always $< 0.6 \text{ m s}^{-1}$. It is encouraging that the mean error remains low even though the later instruments are calibrated using the earlier instruments, and the regional mix of buoy data changes substantially during the period because of the large increase in the number of TAO buoys. We also plot the mean SSM/I—buoy difference separately for observations made during the ascending and descending portions of the orbits.

The most dramatic feature is the downward drift of winds measured by satellite F10 during the years 1993–1996. This same drift is also apparent in global wind speed averages calculated using results from this satellite, as well as in compari-

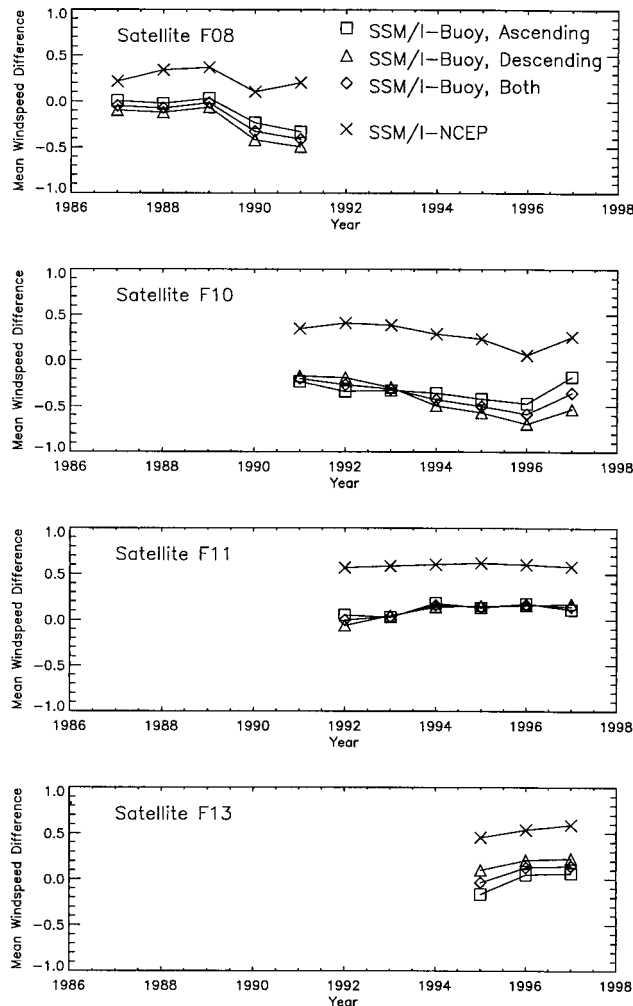


Figure 8. Mean SSM/I—buoy difference and SSM/I—NCEP difference for each satellite and year of valid data. The mean SSM/I—buoy differences are also plotted separately for observations made on the ascending (northward) and descending portions of the orbits. Note the similarities between SSM/I—buoy and SSM/I—NCEP for all satellites and, in particular, the drift in satellite F10. Most of this drift appears to be caused by a drift in descending observations.

sons between satellite F10 and winds speeds modeled by the National Centers for Environmental Prediction *Meissner et al.* [this issue]. The yearly mean SSM/I—NCEP differences are also shown in Figure 8. Note that most of this drift appears to be caused by a drift in descending orbit observations. In Figure 9 we plot weekly means of the SSM/I—buoy wind speed difference for each satellite. In this plot it is apparent that during the time

Table 3. Mean and Standard Deviation of the SSM/I—Buoy Wind Differences for Each Instrument

Satellite Number	Mean ($W_{SSM/I} - W_{buoy}$)	Standard Deviation ($W_{SSM/I} - W_{buoy}$)	Number of Observations
F08	-0.20 ± 0.07	1.39	31233
F10	-0.41 ± 0.05	1.25	88857
F11	0.11 ± 0.05	1.26	86780
F13	0.09 ± 0.05	1.25	46959

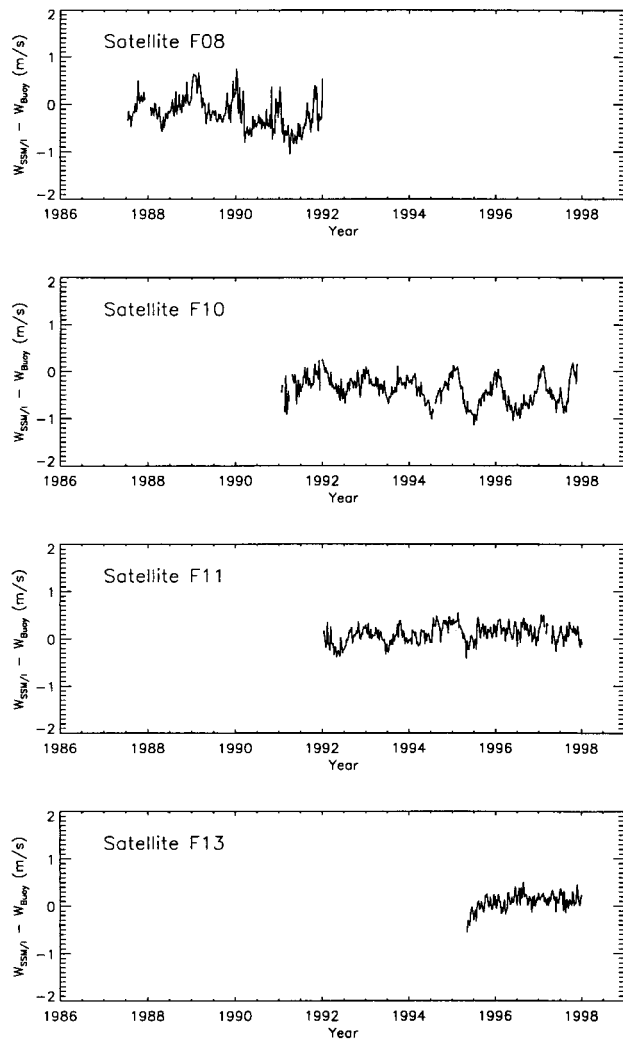


Figure 9. Weekly means of the SSM/I-buoy difference for each satellite. Note the strong seasonal oscillations present for satellite F10 after 1993.

period in which the drift in satellite F10 becomes large, there is also a large seasonal oscillation. This is also the time period in which the orbit of F10 drifted eastward, with the descending equatorial crossing time becoming as late as 1025 LT, more than 4 hours later than the designed crossing time of 0600 LT. This in turn may have led to seasonally modulated orbital fluctuations in satellite temperature due to changes in the amount of time the satellite is exposed to sunlight. We suspect that these fluctuations are responsible for the observed drift in wind speed difference. A similar but smaller drift is observed for F08. This explanation is not all-encompassing since F13 also shows significant differences between ascending and descending orbits, but with the opposite sign, and the F13 wind speed appears to be drifting slightly, even though its orbit is not drifting significantly. The descending crossing time of F13 is almost exactly 0600 LT (0554 LT in December 1998). F11 is also drifting eastward at about 15 min yr^{-1} , with a current (December 1998) descending crossing time of 0725 LT. F11 shows a small ascending/descending difference in 1998, with the same sign as F13.

7. Comparison of Log Correction and Liu Correction

As discussed in section 5, buoy wind speeds are measured using anemometers mounted at a variety of heights. These measured wind speeds need to be converted to wind speeds at a standard height for comparison with SSM/I data. In this section we compare results obtained using two different methods of converting buoy wind speed to 10 m equivalent neutral stability wind. The first method, using a simple logarithmic profile, has been used for all the results in section 6. It neglects differences in atmospheric stability that affect the wind speed profile. We have also implemented a second method developed by *Liu and Tang* [1996] in which the atmospheric stability is taken into account when converting measured wind speeds to 10 m equivalent neutral stability wind. It was hoped that by using this second method of conversion we could significantly reduce the scatter in SSM/I-buoy wind speed differences. We found, instead, that scatter is dominated by other noise sources. We did, however, qualitatively confirm the existence of a stability-induced effect in the satellite data by studying the average error as a function of the difference between sea surface temperature and air temperature.

To illustrate the effects of using the Liu correction on the data obtained from a single satellite-buoy pair, we focus on results from NDBC buoy 46003. At the location of this buoy, 204.06°W longitude, 51.99°N latitude in the Gulf of Alaska, there are significant changes in air temperature leading to times when the atmosphere is stable and other times when the atmosphere is unstable. The large differences in atmospheric stability should make this buoy a good candidate for seeing the benefits of using the Liu correction over the log correction. We have already shown in Figure 2b a scatterplot of the wind speed correction as a function of measured buoy wind speed for this buoy. The height of the anemometer for this buoy is 5 m. It is clear from Figure 2b that both unstable (Liu correction $>$ log correction) and stable (Liu correction $<$ log correction) conditions exist in this data set.

In Figure 10 we plot a scatterplot of SSM/I-buoy difference as a function of measured buoy wind speed; Figure 10 (top) is made using the log-corrected buoy wind speeds, and Figure 10 (bottom) is made using the Liu-corrected wind speeds. There is no obvious difference in the distribution of points for the two plots, and the standard deviation of the difference between SSM/I and buoy wind speeds is only slightly decreased when the Liu correction is used for the buoy. This is not always the case for all buoys; some buoys show an equally slight increase in standard deviation of the difference.

In Table 4 we report the mean difference and standard deviation for each satellite using all valid observations available from all buoys. Mean and standard deviation values are reported for both log-corrected buoy wind speeds and Liu-corrected wind speeds, as well as the difference. All results are in meters per second. The subset of the data used in calculating Table 4 includes only those buoy-satellite collocations for which both the air and sea temperature exists, and thus the Liu correction can be calculated. This requirement excludes about 8% of the data and accounts for the differences in the values presented here and in Table 3.

The effect of using the Liu correction is to shift the mean difference about 0.12 m s^{-1} , with little change in the width of the distribution of the difference. It can also be seen from

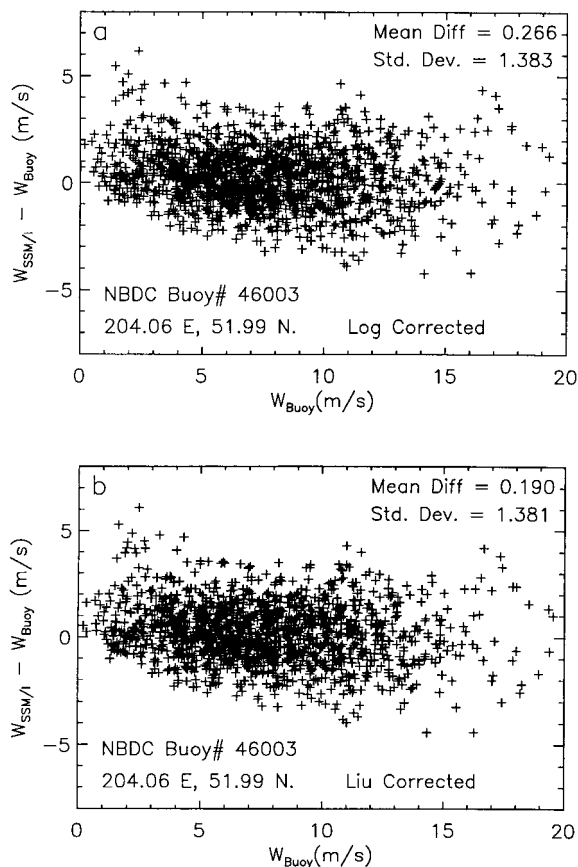


Figure 10. Scatterplot of the difference between SSM/I and corrected buoy wind speeds for satellite F11, buoy 46003 using (a) the logarithmic correction and (b) the Liu correction.

Figure 3 that this average shift is almost completely independent of wind speed.

In an attempt to see whether a shift correlated with atmospheric stability exists we plotted the difference between SSM/I wind speed and buoy wind speed as a function of the difference between the air temperature and sea surface temperature. The atmosphere changes from stable to unstable approximately where this temperature difference changes sign from positive to negative. In Figure 11 we show the binned means of SSM/I-buoy wind speed difference using the Liu correction (Figure 11a) and the

Table 4. Comparison of Means and Standard Deviations of the SSM/I-Buoy Wind Speed Differences Using Different Methods for Correcting Buoy Winds to 10 m

	Log Correction	Liu Correction	Difference
F08			
mean difference	-0.17 ± 0.06	0.30 ± 0.06	-0.13
standard deviation	1.380	1.370	-0.010
F10			
mean difference	-0.44 ± 0.04	-0.54 ± 0.04	-0.10
standard deviation	1.226	1.224	-0.002
F11			
mean difference	0.07 ± 0.04	-0.05 ± 0.04	-0.11
standard deviation	1.230	1.235	0.005
F13			
mean difference	0.05 ± 0.05	-0.07 ± 0.05	-0.12
standard deviation	1.205	1.212	0.007

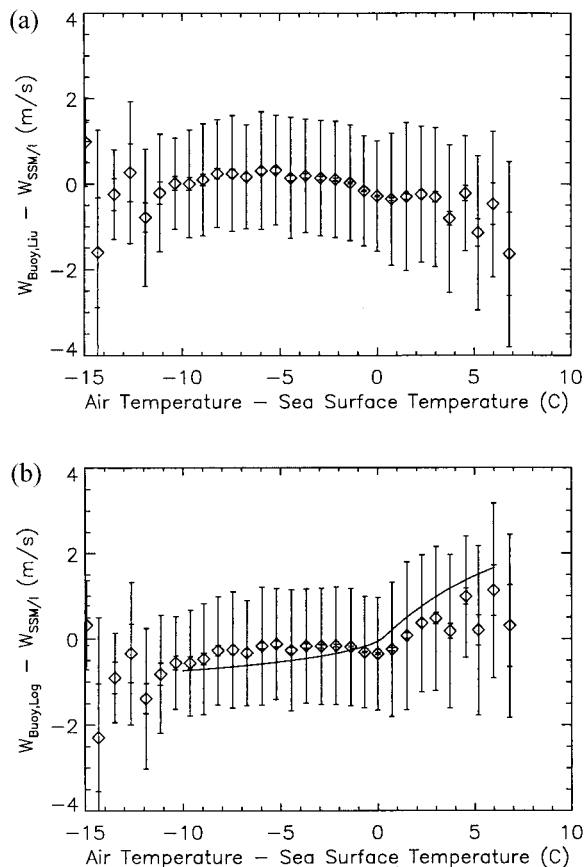


Figure 11. Plot of the difference between mean SSM/I wind speed and buoy wind speed as a function of air-surface temperature difference for satellite F11 and all NDBC buoy winds $<10 \text{ m s}^{-1}$: (a) Liu-corrected buoy wind speeds and (b) log-corrected wind speeds. The kink in Figure 11b near the zero temperature difference is due to effects of atmospheric stability that are ignored by the log correction procedure. The solid line is the difference between Liu correction and log correction for mean conditions.

log correction (Figure 11b) for all NDBC buoy measurements with wind speeds $<10 \text{ m s}^{-1}$. Only NDBC buoys were used because they typically show more variation in air and surface temperature because of their higher-latitude locations, and low winds were chosen because the effects of stability are more pronounced for light winds. In Figure 11b, the Liu-corrected plot, there is no obvious feature as the air-surface temperature difference changes sign. In Figure 11a, the log-corrected plot, there is a obvious kink near zero temperature difference. This is what is expected since the change in atmospheric stability is not taken into account by this correction. The solid line in Figure 11b is the difference between the log correction and the Liu correction for a wind speed of 6.3 m s^{-1} and a sea surface temperature of 18.4°C . These are the average values of these parameters across the low-wind NDBC satellite F11 data set. The relative humidity was assumed to be 80%, and the pressure was assumed to be 1015 mbar.

In this section we have established that the main effect of using the more sophisticated Liu correction to convert measured buoy winds to equivalent neutral density winds is to offset all measurements by a small $\sim 0.12 \text{ m s}^{-1}$ correction factor. The distribution of SSM/I-buoy wind speed differences

Table 5. Estimated Error Budget for SSM/I-Derived Wind Speeds

Error Source	Estimated Contribution to Standard Deviation, m s^{-1}
Atmospheric model	0.51
Wind direction	0.35
Radiometer noise	0.53
Sampling and mismatch	0.94
Total predicted	1.24
Total observed	1.25 to 1.38

is almost unaffected. The effects of stability on buoy wind speed are only clearly seen when a large number of collocations are averaged and plotted as a function of air-surface temperature difference. Although it is more rigorously correct to use the more complicated Liu correction, the use of the simpler log correction procedure when calibrating the Wentz algorithm for processing of SSM/I data did not lead to errors that are large on the scale of other noise sources involved in the measurement.

8. Error Analysis

In the preceding sections we have made a detailed comparison between wind speeds measured by buoys and those derived from SSM/I observations. In this section we will summarize the estimated error budget of the SSM/I and buoy wind speed products and assign an estimated error to the wind speed reported by the SSM/I instrument.

In many previous studies the wind speeds measured by in situ measurements have been assumed to be the “true” wind speeds, and all errors have been assigned to the remotely sensed wind speeds. This is philosophically unappealing since buoy and satellites measure two different quantities. Buoys measure the time average of the wind speed over a short time (typically <10 min) at a single point. Satellites, on the other hand, make a nearly instantaneous measurement of the wind averaged over the spatial footprint of the satellite. Since most researchers would agree that the goal of the satellite program is to provide global measurements of synoptic-scale geophysical parameters, it is in some sense “unfair” to assign all the differences between satellite and buoy measurements to errors in the satellite measurement. Instead, we view the satellite and buoy measurements both to be estimates of the synoptic scale wind field. With this view, part of the standard deviation of the difference between buoy and satellite measurements can be assigned to sampling errors in the buoy estimate of the synoptic wind field. The estimated error of the satellite measurement inferred from the buoy-satellite wind speed difference can then be reduced.

The error budget for the SSM/I instrument and collocation and sampling errors are discussed in detail by Wentz [1997]. These previous results are summarized in the first five entries in Table 5. From Table 5 we can see that the largest contribution to the observed standard deviation of the SSM/I-buoy difference is due to sampling and mismatch error, with significantly smaller error due to radiometer noise in the SSM/I instrument, to unretrieved wind direction effects, and to errors in the model used to retrieve and remove atmospheric effects. The quadrature sum of the predicted effects, 1.24 m s^{-1} , is in good agreement with the measured standard deviation, which

ranges from 1.25 to 1.39 m s^{-1} for the four satellites under consideration. As argued above, we can subtract the sampling and mismatch error in quadrature from the observed error to obtain an estimated standard deviation of the error ranging from 0.82 to 1.02 m s^{-1} . These value represents an estimate of the standard deviation of the difference between the reported SSM/I wind speed and the actual wind field, averaged over an SSM/I pixel.

9. Conclusions

We have performed a detailed comparison between SSM/I-derived wind speeds and those measured using moored buoys. This is the first such comparison that has compared wind speed values from each of the four SSM/I satellites that have been accurately cross calibrated to a large sample of buoy measurements to date. The results are very encouraging. Mean differences between SSM/I winds and buoy winds are $<0.5 \text{ m s}^{-1}$, and the standard deviation of the difference is around 1.3 m s^{-1} . No large regional or wind speed-dependent biases were found. Since the SSM/I data used for this study were those generally available to all researchers via the Internet, these data can now be used with greater confidence for scientific studies.

We have also compared two different methods of converting observed buoy wind speeds to the neutral stability winds that are more directly observed by microwave remote sensing. We found that there is little difference between a simple logarithmic scaling and a more complicated algorithm that takes into account estimates of the atmospheric stability. For our SSM/I-buoy data set the only appreciable difference between the two methods was a constant bias of a few tenths of a meter per second.

Acknowledgments. The authors would like to thank Michael J. McPhaden, director of the TAO Project Office, for providing data from the TAO buoy array and the National Data Buoy Center for providing the NDBC buoy data. We are also thankful to the Defense Meteorological Satellite Program for making the SSM/I data available to the civilian community. We are very grateful for continuing support from NASA. This research was funded by Oregon State University subcontract NS070A-01 under NASA research grant NAG5-6642.

References

- Ardizzone, J., R. Atlas, J. C. Jusem, and R. N. Hoffman, Application of SSM/I wind speed data to weather analysis and forecasting, paper presented at 15th Conference on Weather Analysis and Forecasting, Am. Meteorol. Soc., Norfolk, Va., 1996.
- Boutin, J., and J. Etcheto, Consistency of Geosat, SSM/I, and ERS-1 global surface wind speeds: Comparison with in situ data, *J. Atmos. Oceanic Technol.*, *13*, 183–197, 1996.
- Boutin, J., L. Siefridt, J. Etcheto, and B. Barnier, Comparison of ECMWF and satellite ocean wind speeds from 1985 to 1992, *Int. J. Remote Sens.*, *17*, 2897–2913, 1996.
- Busalacchi, A. J., R. M. Atlas, and E. C. Hackert, Comparison of special sensor microwave imager vector wind stress with model-derived and subjective products for the tropical Pacific, *J. Geophys. Res.*, *98*, 6961–6977, 1993.
- Chou, S.-H., R. M. Atlas, C.-L. Shie, and J. Ardizzone, Estimates of surface humidity and latent heat fluxes over oceans from SSM/I data, *Mon. Weather Rev.*, *123*, 2405–2425, 1995.
- Chou, S.-H., C.-L. Shie, R. M. Atlas, and J. Ardizzone, Evaporation estimates over global oceans from SSM/I data, paper presented at Eighth Conference on Satellite Meteorology and Oceanography, Am. Meteorol. Soc., Atlanta, Ga., 1996.
- Chou, S.-H., C.-L. Shie, R. M. Atlas, and J. Ardizzone, Air-sea fluxes

- retrieved from special sensor microwave imager data, *J. Geophys. Res.*, *102*, 12,705–12,726, 1997.
- da Silva, A. M., C. C. Young-Molling, and S. Levitus (Eds.), *Atlas of Surface Marine Data 1994* vol. 1, *Algorithms and Procedures*, NOAA Atlas NESDIS, vol. 6, Natl. Oceanic and Atmos. Admin., Silver Spring, Md., 1994.
- Deblonde, G., and N. Wagneur, Evaluation of global numerical weather prediction analyses and forecasts using DMSP special sensor microwave imager retrievals, 1, Satellite retrieval algorithm intercomparison study, *J. Geophys. Res.*, *102*, 1833–1850, 1997.
- Deblonde, G., W. Yu, L. Garland, and A. P. Dastoor, Evaluation of global numerical weather prediction analyses and forecasts using DMSP special sensor microwave imager retrievals, 2, Analyses/forecasts intercomparison with SSM/I retrievals, *J. Geophys. Res.*, *102*, 1851–1866, 1997.
- Esbensen, S. K., D. B. Chelton, D. Vickers, and J. Sum, An analysis of errors in special sensor microwave imager evaporation estimates over global oceans, *J. Geophys. Res.*, *98*, 7081–7101, 1993.
- Gilhousen, D. B., A field evaluation of NDBC moored buoy winds, *J. Atmos. Oceanic Technol.*, *4*, 94–104, 1987.
- Halpern, D., Validation of special sensor microwave imager monthly-mean wind speed from July 1987 to December 1989, *IEEE Trans. Geosci. Remote Sens.*, *31*, 692–699, 1993.
- Hayes, S. P., L. J. Magnum, J. Picaut, and K. Takeuchi, TOGA-TAO: A moored array for real-time measurements in the tropical Pacific ocean, *Bull. Am. Meteorol. Soc.*, *72*, 339–347, 1991.
- Hollinger, J., R. Lo, G. Poe, R. Savage, and J. Pierce, The special sensor microwave/imager user's guide, NRL technical report, pp. 1–120, Nav. Res. Lab., Washington, D. C., 1987.
- Ledvina, D. V., and J. Pfaendtner, Inclusion of special sensor microwave/imager (SSM/I) total precipitable water estimates into the GEOS-1 data assimilation system, *Mon. Weather Rev.*, *123*, 3003–3015, 1995.
- Liu, W. T., and W. Tang, Equivalent neutral wind, Jet Propul. Lab., Pasadena, Calif., 1996.
- Mangum, L. J., H. P. Freitag, and M. J. McPhaden, TOGA-TAO array sampling schemes and sensor evaluations, paper presented at Oceans '94 Ocean Space Adv. Technol. Eur. Show, Inst. of Electr. and Electr. Eng., Brest, France, 1994.
- McPhaden, M. J., The tropical atmosphere ocean (TAO) array is completed, *Bull. Am. Meteorol. Soc.*, *76*, 739–741, 1995.
- Meissner, T., D. Smith, and F. Wentz, A 10 year intercomparison between collocated Special Sensor Microwave Imager oceanic surface wind speed retrievals and global analyses, this issue.
- Peixoto, J. P., and A. H. Oort, *Physics of Climate*, Am. Inst. of Phys., Woodbury, N. Y., 1992.
- Waliser, D. E., and C. Gautier, Comparison of buoy and SSM/I-derived wind speeds in the tropical Pacific, *TOGA Notes*, *12*, 1–7, 1993.
- Wentz, F., A well-calibrated ocean algorithm for SSM/I, *J. Geophys. Res.*, *102*, 8703–8718, 1997.
-
- C. A. Mears, D. K. Smith, and F. J. Wentz, Remote Sensing Systems, 438 First Street, Suite 200, Santa Rosa, CA 95401. (mears@remss.com)

(Received October 12, 1999; revised May 28, 2000; accepted November 29, 2000.)

